AIP | Review of Scientific Instruments

Mapping temperatures and temperature gradients during flash heating in a diamond-anvil cell

Zhixue Du, George Amulele, Laura Robin Benedetti, and Kanani K. M. Lee

Citation: Rev. Sci. Instrum. **84**, 075111 (2013); doi: 10.1063/1.4813704
View online: http://dx.doi.org/10.1063/1.4813704
View Table of Contents: http://rsi.aip.org/resource/1/RSINAK/v84/i7
Published by the AIP Publishing LLC.

REVIEW OF SCIENTIFIC INSTRUMENTS **84**, 075111 (2013)

Mapping temperatures and temperature gradients during flash heating in a diamond-anvil cell

Zhixue Du,[1,a] George Amulele,[1] Laura Robin Benedetti,[2] and Kanani K. M. Lee[1,b]
[1]*Department of Geology and Geophysics, Yale University, New Haven, Connecticut 06511, USA*
[2]*Lawrence Livermore National Laboratory, Livermore, California 94550, USA*

(Received 15 March 2013; accepted 27 June 2013; published online 19 July 2013)

Here, we couple two-dimensional, 4-color multi-wavelength imaging radiometry with laser flash heating to determine temperature profiles and melting temperatures under high pressures in a diamond-anvil cell. This technique combines the attributes of flash heating (e.g., minimal chemical reactions, thermal runaway, and sample instability), with those of multi-wavelength imaging radiometry (e.g., 2D temperature mapping and reduction of chromatic aberrations). Using this new technique in conjunction with electron microscopy makes a powerful tool to determine melting temperatures at high pressures generated by a diamond-anvil cell. © *2013 AIP Publishing LLC*. [http://dx.doi.org/10.1063/1.4813704]

INTRODUCTION

With the invention of the laser-heated diamond-anvil cell (DAC), simultaneous high pressures and high temperatures can be achieved while also visually observing and optically probing the sample. This technique has facilitated large advances in physics, chemistry, geology, and materials science.[1] Investigation of material behavior at extreme thermodynamic conditions requires accurate characterization of the high pressures and high temperatures. As such, there have been many studies designed to quantify the high-temperature and high-pressure conditions within the laser-heated DAC (e.g., Refs. 2–12). One of the most significant challenges stems from the nature of diamonds themselves: diamond is an excellent thermal conductor and encourages steep thermal gradients. Temperature gradients in laser-heated samples can reach $\sim 10^2$ K/μm, thus quantifying these gradients is a step toward accurately determining the thermodynamic state of the sample. In general, as pressure and temperature increase, the gradients in these quantities also increase. Even so, the diamond-anvil cell has become the tool of choice for obtaining high pressures under static conditions due to its simple and flexible design, and the optical access afforded by the diamond anvils over a wide range of the electromagnetic spectrum. Consequently, the need to accurately characterize gradients in pressure and temperature within the laser-heated DAC remains.

Among the most fundamental problems undertaken in high-pressure science is the determination and measurement of melting temperatures. A variety of methods have been used to identify the onset of melting; some are direct, but most are proxies.[13] Fluid motion during heating was used to identify melting in early studies[14–16] and has been claimed to be the most efficient way to determine melting temperature due to the direct observation of the loss of rigidity, a fundamental characteristic of a fluid.[13] However, this becomes increasingly subjective and impractical at temperatures above ∼3000 K as bright thermal emissions obscure the observation of the onset of motion due to lack of adequate contrast across the hotspot.[13] Additionally, at high pressures, fluid motion may become more sluggish further complicating observation.[17] Therefore, fluid motion may not be an optimal method to identify melting.

The quenching of initially crystalline material into a glass upon turning off the laser is also an effective, however, indirect way to identify melting, and is restricted to glass-forming materials.[18,19] For lower mantle minerals such as (Mg, Fe)SiO_3, it is difficult to obtain a glass structure despite the fast quench rate (10^6–10^7 K/s) in the diamond-anvil cell.[13] In practice, identifying small amounts of glass after heating is far from trivial; as such, this method is rarely used. Conceptually similar, quench texture is widely used in large-volume press experiments as a proxy to identify melting (e.g., Ref. 20). While this method has also been used in a few laser-heated diamond-anvil cell experiments,[16,21] observation of texture changes in the DAC is complicated by other mechanisms that may also cause textural changes such as solid-state transformations, especially when a silicate glass is used as a starting material. In addition, it is not straightforward to identify texture changes after laser heating, especially when the area at peak temperature is small due to the small hotspot and significant temperature gradients.

The correlation between temperature and laser power has also been widely used in many DAC experiments as a proxy for melting (e.g., Refs. 22 and 23). This change in slope for the temperature-laser power relationship has been interpreted as the absorption of latent heat upon melting. Unfortunately, this interpretation is flawed and mechanism poorly understood. It has also been pointed out that a change of slope might be simply due to less efficient heating at high temperature caused by high radiative energy loss,[13] or increased thermal conductivity of the melt as compared to the solid.[24,25] Additionally since laser absorbers, such as W or Re foils, and

---

[a] Author to whom correspondence should be addressed. Electronic mail: zhixue.du@yale.edu

[b] Author to whom correspondence should be addressed. Electronic mail: kanani.lee@yale.edu

pressure media (e.g., MgO, Al_2O_3, or Ar) are also used when heating the samples in these studies, it is not clear whether the slope changes observed in the temperature versus power curve are caused by melting of the sample itself; (b) melting of laser absorber; or (c) partial melting of the sample, pressure medium, and laser absorber.

Much progress of improving the overall laser heating technique has been made over the last decade. For example, double-sided laser heating has been introduced (e.g., Ref. 26), which can reduce temperature gradients toward the diamond anvils. Combined with intense synchrotron x-ray sources, melting curves can be measured by x-ray diffraction (e.g., Ref. 27), although these are challenging even with reduced temperature gradients. Also many studies have focused on understanding and quantifying the accuracy of temperature measurements (e.g., Refs. 2–4, 12, and 28). Additionally, with the advent of multi-wavelength imaging radiometry (i.e., "4-color" temperature measurement), measuring two-dimensional temperature gradients has become possible for laser-heated samples, both at ambient pressure and at high pressures in a DAC.[5] This is an ideal way to quantify temperature distribution in the laser-heated DAC, and the method eliminates (or at least substantially reduces) chromatic aberrations that may have marred previous temperature measurements. This method also yields a measure of the emissivity of a sample. As emissivity has been claimed to jump (change discontinuously) upon melting,[5,29] this technique presents another proxy for determining melting conditions. Also recently developed, is the method of flash heating in order to minimize sample instability, thermal runaway, and chemical reactions.[30] We show that these two techniques can be combined effectively after minor revision of the original 4-color design,[5] to create a powerful new technique of *in situ* 2D temperature measurements under high quasi-hydrostatic pressures and *ex situ* texture and composition analysis of quenched samples.

METHODS

Optical setup

In order to measure temperatures of flash-heated samples where the duration of the laser heating is of order 10 ms, it was necessary to revise the multi-wavelength imaging design[5] (Fig. 1). In the original design, each of the four wavelengths had associated mirrors that individually allowed the focusing of each wavelength image on to the CCD (labeled "M3" in Fig. 2 of Campbell[5]). Although these mirrors do allow a precise change in the light path for each individual wavelength, they additionally decreased the light intensity by a factor of four for each wavelength path. As the focal length of the achromat lens used in our design only varies slightly between the wavelengths used in our 4-color system ($\sim$0.1% = <1 mm out of 750 mm), the increased flux gained by the removal of these mirrors outweighs their focusing ability. Additionally, we removed one of the cube beam splitters from the design as this became unnecessary without the extra mirrors. In fact, images were much sharper without the extra optics and more easily aligned.

Another change we made to the original design was to replace the pellicle beam splitter ("BS1" in Fig. 1 that splits the light between the spectroradiometer and imaging radiometer systems in Campbell[5]) with a cube beam splitter. We found the pellicle beam splitter to show significant wavelength dependent thin-film interference fringes that are not present with the cube beam splitter. Although pellicle beam splitters are handy in optical designs (e.g., we use them to help illuminate the sample when not collecting temperature measurements), we remove them when measurements are taken due to their very sensitive wavelength-dependent interference. Another added benefit of removing the pellicle beam splitter, is that when present, it cuts the laser power by $\sim$50%, thus decreasing the efficiency of the laser.

Another necessary change we found was in the choice of narrow-band filters. As precise imaging is the goal of our present design, ghost reflections must be avoided. We found that with traditional narrowband filter designs with multiple coatings, ghosting (i.e., faint reflections from each layer) is not easily avoided. Consequently, we used hard-coated narrowband filters that essentially negated any ghost reflections due to the filters themselves: see the caption of Fig. 1 for details.

Prior to the removal of these optics, the sharpness of image did not appear to change with up to 5 mm increase or decrease in the length of the individual light paths. The sharper image due to the increased flux, simplification of the optical design, and removal of ghosting narrow-band filters, make for a much sharper image in all four colors.

Additionally, we monitor the laser flash pulse shape and resulting thermal emission by photodiodes (Thorlabs DET36A, PDA36A, respectively) and oscilloscope (Agilent U2702A). Only measurements that had a flat laser flash pulse and subsequent quick rise time ($\sim$1 ms) to steady-state thermal emission are included in this paper (e.g., Ref. 30). It is important to note that superheating and/or runaway heating is possible and is sample and laser pulse dependent, thus monitoring both the laser pulse and thermal emission is necessary. We note and discuss below in detail that Pt heating stability only occurs after several seconds of continuous (CW) heating.

DATA ANALYSIS

As described by Campbell,[5] we record simultaneous images of the thermal emission at each of the four wavelengths. As described below, these four images are then spatially registered to produce two-dimensional maps of temperature and relative emissivity after correction for the relative response and background of each image.

In addition to enclosing the entire 4-color optical system in a black box, we collect and subtract a dark image (identical collection time and conditions, but with the CCD shutter closed) to account for any external light sources. For completeness, we also minimize inherent detector noise by using a thermo-electrically cooled CCD detector (SBIG ST-402ME). Consequently, external light leaks and instrument noise are small compared to the dominant background signal and scatter from the many surfaces in the optical setup. This signal is unavoidable: in order to produce four narrow-wavelength

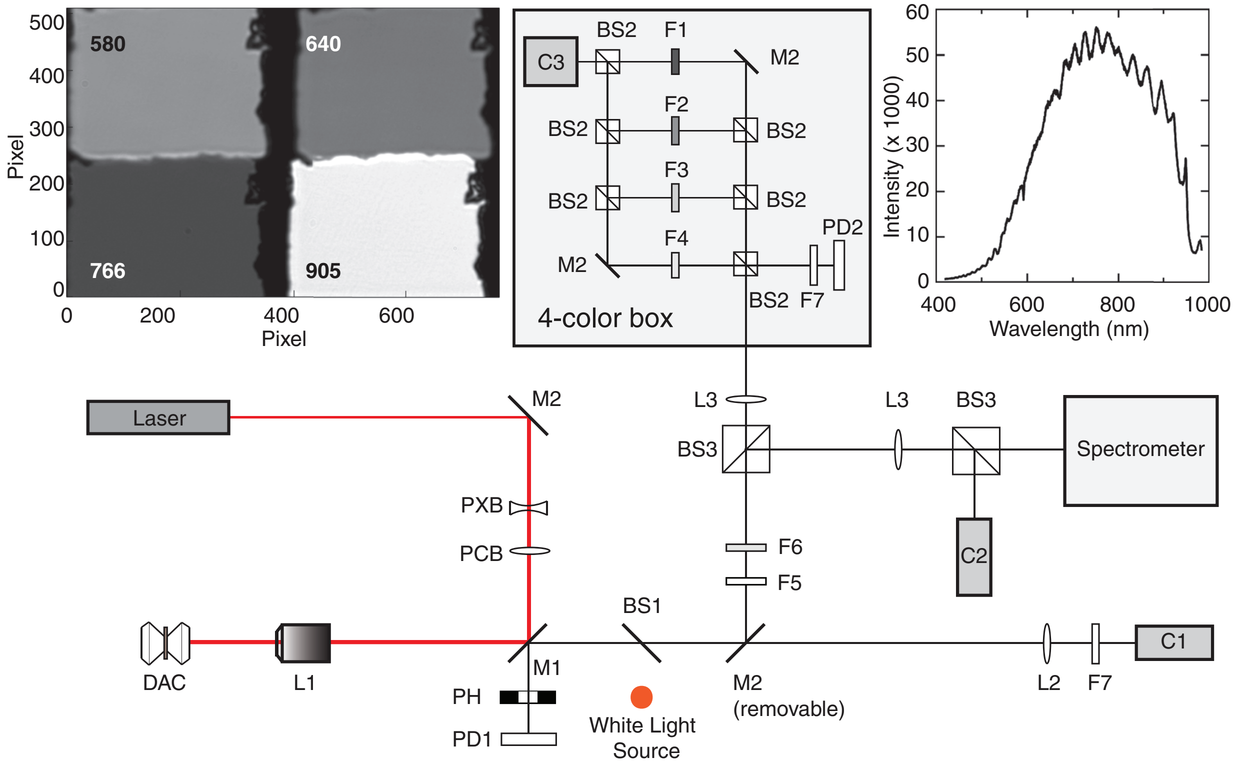

FIG. 1. Laser-heating and 4-color multi-wavelength radiometry optical layout for single-sided laser heating. L1: Mitutoyo NIR 5X Objectives; DAC: Diamond-Anvil Cell; Laser: SPI 100 W water-cooled fiber laser; L2: Thorlabs AC254-200-B Achromat NIR lens 200 mm; L3: Thorlabs AC508-750-B Achromat NIR lens 750 mm; M1: Newport 10QM20HM.15 laser mirrors; M2: Thorlabs PF10-03-P01 silver mirrors; F1: Edmund Optics 65184 905 nm narrow-band filter; F2: Edmund Optics 65177 766 nm narrow-band filter; F3: Edmund Optics 65168 640 nm narrow-band filter; F4: Edmund Optics 65161 580 nm narrow-band filter; F5: Edmund NT86-123 notch filter; F6: Thorlabs neutral density filters NEK01; F7: Thorlabs FGS 900 glass filter; BS1: Thorlabs BP145B2 Pellicle beam splitter (removed during heating and calibration); BS2: OptoSigma 039-0260 cube beam splitters; BS3: OptoSigma 039-0265 cube beam splitters; PH: Iris diaphragm used as adjustable pin hole (Thorlabs ID25); PD1: Thorlabs photodiode DET36A; PD2: Thorlabs photodiode PDA36A; photodiodes connected to Agilent U2702A 200 MHz oscilloscope (not shown); PCB: CVI Laser PCB-25.4-51.5-C-1064 concave lens, PXB: CVI Laser PXB-25.4-65.4-C-1064 Achromat convex lens; Spectrometer: Princeton Instruments Acton Advanced SP2300A Spectrometer equipped with PIXIS 100 CCD; C1: Hitachi CCD; C2: Mightex CGE-C013-U camera; C3: SBIG ST-402ME. The entire "4-color box" is enclosed in a black box to minimize any stray light. The removable M2 mirror is mounted on a magnetic kinematic mount to ensure ease of use and alignment when switching between cameras. The raw system response data for the 4-color and spectrometer are given in top left and top right corners, respectively. The raw average counts and standard deviation for each wavelength in the 4-color system is as follows: 580 nm: 11 753 (172); 640 nm: 60 164 (587); 766 nm: 33 435 (325); and 905 nm: 24 546 (361). The system responses correspond to a setup without a neutral density filter.

images, more than 99% of the thermally emitted light is rejected and left to produce a (nearly) uniform radiation field within the optical box. This background is measured in a region that does not overlap the hotspot images and removed as a uniform level from the entire frame. It is this background, and not the camera itself, that ultimately limits the useful dynamic range of the measurement and consequently the lower limit of temperature from a single image:[5] ~1200 K provided the duration of the measurement and heating is long, > ~1 s (CW heating). When the heating duration is short (e.g., flash heating for 10s of ms), temperatures as low as ~2500 K are routinely measureable. Lower temperatures can be measured with longer flash heating durations or by removing one beam splitter from the optical setup, thus sacrificing either one of the multiple wavelengths or simultaneity with the spectrometer temperature measurements.

The optical response of the system was calibrated for each of the four wavelength bands using a 45 W standard coil lamp whose irradiance, I(λ), is traceable to NIST standards (Newport Corp. 63358). The lamp was placed behind a 100 μm × 150 μm pinhole in the focal plane of the microscope in order to project four well-separated images onto the CCD camera. The distance the lamp was placed behind the pinhole did not significantly change the resulting measurements, thus to increase the counting statistics, the lamp was placed at a nearby distance of ∼ 20 cm behind the pinhole. Each image is large enough that its central portion is free of diffraction edge effects: the average value over this central region, normalized by the known irradiance, was used as the response of the entire system for each wavelength band. Using an averaged response value prevents a multiplicative noise effect, and is estimated to add a minor systematic error of <1% relative to independently calibrating each pixel location.

We also present spectroradiometric measurements collected on a Princeton Instruments Acton Advanced SP2300A Spectrometer equipped with PIXIS 100 CCD (Fig. 1). The wavelength-dependent response of the spectrometer's optical system is calibrated at the same time as the 4-color measurement system over the full spectral range of the spectrometer (~400–1000 nm), which is centered at 700 nm. Wavelength is calibrated on the spectrometer using a Ne lamp. Temperatures are determined by spectroradiometry in the spectral range between ∼560 and 860 nm, as explained below. For completeness, we show the system responses for both systems in Fig. 1.

Spatial correlation and temperature determination

Temperature determination requires an intensity measurement for each wavelength at each location, and this requires that the four images be accurately registered to each other. This is, of course, especially important when samples are small and temperature gradients are large, as in the laser-heated DAC. We used image correlation methods to register the four images, linearly interpolating to achieve coincidence within 0.2 pixels (∼0.1 μm). We correlated the images so that the most intense image (highest signal to noise) was not interpolated. The correlation coefficient R is defined as

$$R = \frac{\sum_{i=1}^{n}(X_i - \bar{X})(Y_i - \bar{Y})}{\sqrt{\sum_{i=1}^{n}(X_i - \bar{X})^2}\sqrt{\sum_{i=1}^{n}(Y_i - \bar{Y})^2}},$$

where X and Y are two variables, in this case intensity and shape. $R = 1$ is achieved for perfectly correlated images, while uncorrelated images yield $R = 0$. Data were rejected if all three correlation coefficients, R, were not greater than 0.98. Typically, $R > 0.99$ are achieved with this system and lower R values can be indicative of low signal (e.g., low temperatures of Pt melting), poor optical quality, poor alignment, or a combination of these.

Once the four images are intensity corrected and spatially correlated, the intensities in each of the four images provide a set of pixel-by-pixel spectra that we fit to the Wien function

$$Wien = \frac{k}{hc}\ln\left[\frac{2\pi hc^2}{I\lambda^5}\right],$$

which can be rewritten as

$$Wien = \frac{k}{hc}\ln\left[\frac{2\pi hc^2}{I\lambda^5}\right] \approx \frac{1}{\lambda}\frac{1}{T} - \frac{k}{hc}\ln\varepsilon,$$

so that the temperature is determined from the slope of a weighted linear least-squares fit. I is the intensity of emission, ε is the sample emissivity, λ is wavelength, and T is temperature. The constants π, h, c, and k are pi, Planck's constant, the speed of light, and Boltzmann's constant, respectively. We assume the gray-body approximation, in which the sample emissivity is assumed to be independent of wavelength, so that the four intensities are fit to two adjustable parameters: temperature and gray-body emissivity. This approximation is warranted for the materials investigated here, at least at room pressures, as the emissivity is only weakly dependent on wavelength.[4] The resulting error using a gray-body approximation ranges from less than 1% for W to less than 5% for Pt,[4] although the effect of pressure on wavelength-dependent emissivity is unknown. The Wien approximation introduces negligible error below 4000 K as compared to a Planck fit[15]

$$I = \varepsilon\frac{2\pi hc^2}{\lambda^5}\frac{1}{e^{hc/\lambda kT} - 1}.$$

We use the Wien approximation not only for convenience but as there are only 4 wavelength bands, rather than a full spectra as is typical of spectroradiometric measurements, any approximation more complex is not statistically supported. Subsequently, the linear fit is sufficient and the goodness of the gray-body Wien approximation yields an uncertainty that is typically 5%. Additional uncertainties stem from the following sources: calibrations and corrections (<1%), spatial resolution of melt bleb texture and corresponding temperature map (∼2%), and differences between multiple measurements (∼1%). Thus, for a melting temperature measurement of 4000 K using the 4-color system, our uncertainties are ∼300 K. We assume that across each hotspot, the relative uncertainties remain constant.

Melt identification

To effectively use the temperature map to infer melting temperatures, we used scanning electron microscopy (SEM) images in either backscattered electron (BSE) or secondary electron (SE) modes. The morphology of the surface changes upon heating and melting (Fig. 2). We observe recrystallization and grain growth on samples that are heated, but at temperatures lower than the melting temperatures. For temperatures above the melting temperature, we observe melt "blebs." The melting temperature is determined by tracing the perimeter of the melt bleb from the SEM image and superimposing the perimeter on to the temperature map. To do so, care must be taken in determining the pixel resolution of the CCD camera and the optical setup of the 4-color system (see below). This method is completely consistent with measurements taken below melting where no melt texture is observed (Figs. 4 and 7).

While it is ideal to perform reversal experiments to determine the kinetics of melting, we note the irreversibility of

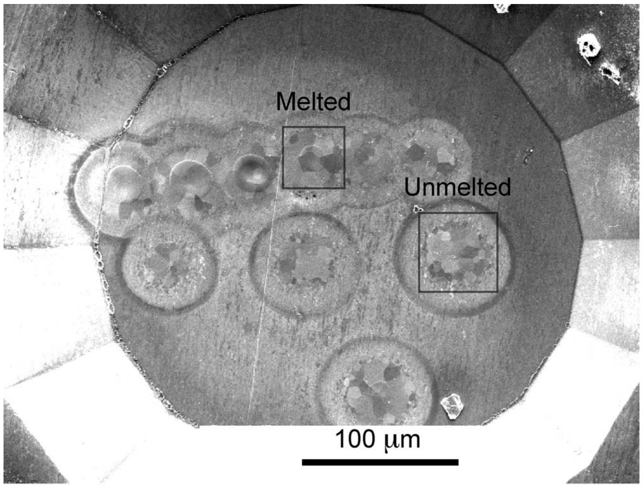

FIG. 2. SEM image of W gasket after flash heating at various laser power at room pressure. There are 10 different regions that were heated, five of which melted. Two regions are boxed and are shown in detail in Figs. 3(c) ("melted") and 4(c) ("unmelted"). Note the recrystallization and grain growth of the W where the material was heated but unmelted, and the round bleb regions that were melted. (Note that the region compressed to be flat and uniform is the area within the 16-sided polygon.)

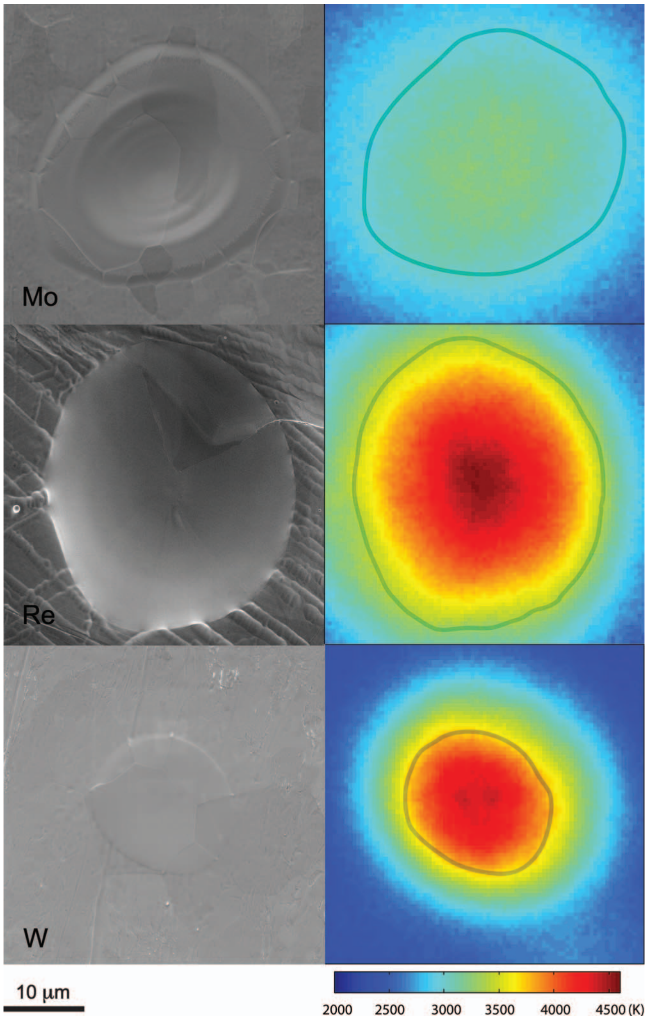

FIG. 3. (Left) SEM images and (right) corresponding temperature maps of melted samples of (a) Mo, (b) Re, and (c) W. The outlines shown on the temperature maps correspond to the melt bleb perimeters in the SEM images.

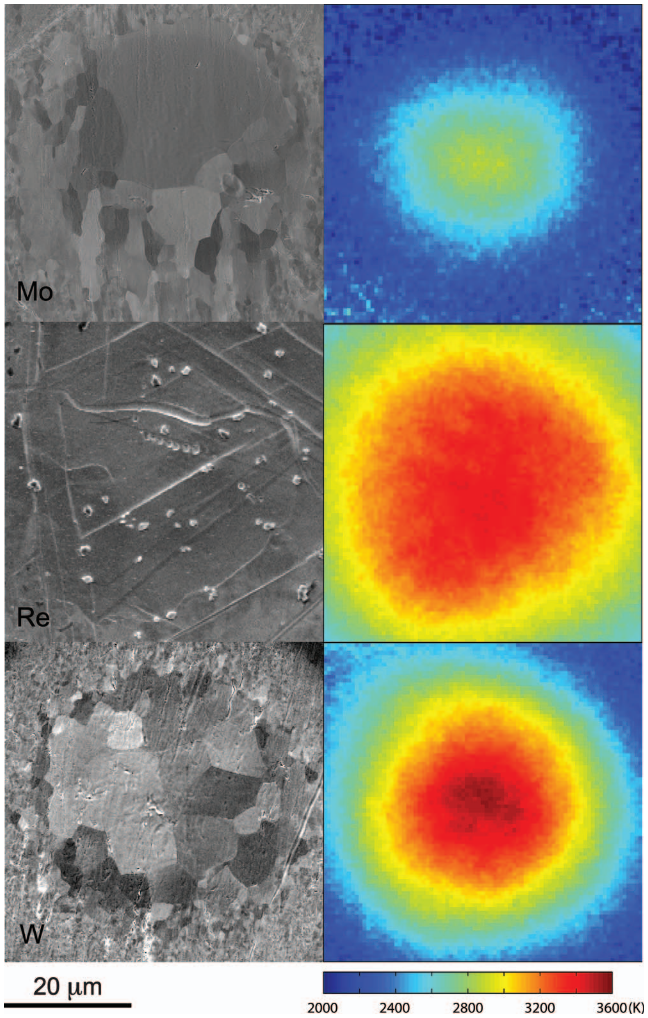

FIG. 4. (Left) SEM images and (right) corresponding temperature maps of unmelted samples of (a) Mo, (b) Re, and (c) W. Note the strong recrystallization of the heated areas especially visible in Mo and W.

this technique which combines flash melting, 2D temperature maps, and *ex situ* electron microscopy for melt identification. The experimental technique is not reversible, as it requires the recovery of the texture while molten. This appears to not be a problem for the materials investigated in this study. Since multiple flash-heated spots can be taken on a given sample foil (e.g., Fig. 2), whether at room pressure or high pressure, several measurements above and below the melting temperature constrain the melting temperatures as well as the possible presence of superheating. As such, we find that if superheating is present, it is of order 100 K (Figs. 2–4 and 7), similar to what has been observed previously.[30] Nonetheless, superheating could be significant for other samples including multi-component systems, silicates, alloys, etc.

Although less important for pure substances such as the metals we use in this study, SEM or electron probe microanalysis (EPMA) can also generate compositional maps of quenched samples, thus flash-heated samples can have all of the relevant thermodynamic parameters known: pressure, temperature, and chemistry in addition to morphology.

Pixel calibration and magnification

In order to compare SEM images with the temperature maps, we carefully calibrated the magnification of our optical system(s) using a reticule with 10 μm divisions. The 4-color camera (C3, Fig. 1) was found to image 0.48 μm at the object plane per 9 μm pixel, while the spectrometer images at 1.07 μm at the object plane per 20 μm pixel. Although the 750 mm achromat lens imposes magnification, the difference in the pixel resolution stems from the inherently different physical pixel sizes between cameras (9 × 9 μm versus 20 × 20 μm for C3 and spectrometer cameras (Fig. 1), respectively).

EXPERIMENTS

Room-pressure flash melting

Four transition metals (Pt, Mo, Re, W) of known ambient pressure melting temperatures were used to verify our 4-color temperature measurement system. These metals were chosen to span the typical temperature range of laser heating used in the DAC (~2000–4000 K). For Mo, Re, and W,

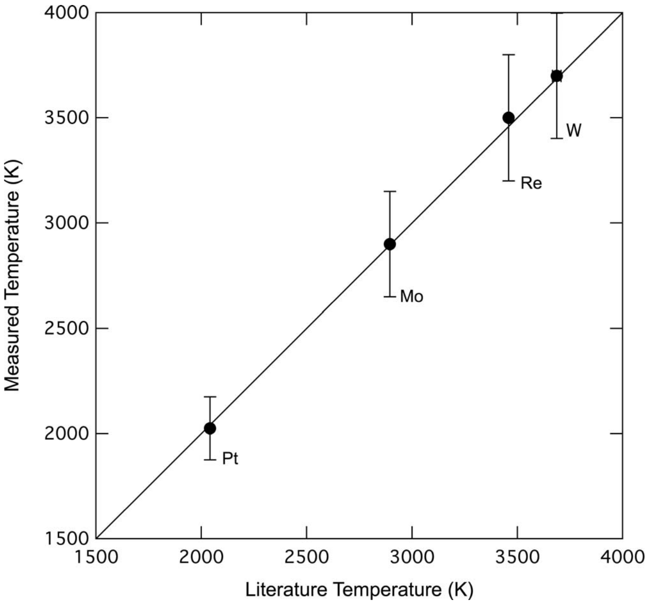

FIG. 5. Measured melting temperatures of Pt, Mo, Re, and W by 4-color pyrometry as compared to literature values. Uncertainties given are due to multiple measurements as well as uncertainties in the calibration. Literature melting temperatures are 2041 K, 2895 K, 3458 K, and 3687 K for Pt, Mo, Re, and W, respectively. Uncertainties in literature values are ∼5–20 K and are plotted, although are generally smaller than the symbol size. The line shows the 1:1 relationship.

a single 20 ms laser pulse of varying laser power was used to heat each foil. Each of the cleaned metal foils was compressed between two diamond anvils in order to achieve a flat and uniform thickness ready for heating. Due to the potential reactivity of Mo, Re, and W under high temperatures, the foil was continuously purged with argon gas in order to minimize any reactions between the air and metals. Energy-dispersive x-ray spectra (EDS) were taken on quenched samples to check for oxidation and none was found, consistent with a previous flash-melting study.[30] Multiple measurements (Fig. 2) at laser powers yielding temperatures above (Fig. 3) and below (Fig. 4) melting temperatures were taken. We obtained remarkable agreement between our melting temperatures and literature values (Fig. 5).

In our laser-heating optical setup (Fig. 1), we also use spectroradiometry, the traditional way to measure temperatures, and find very good agreement of peak temperature determination as well as 1D temperature profile of the hotspot as imaged on to the narrow slit (50 μm, corresponding to ∼2.6 μm sliver of the hotspot) of the spectrometer (Fig. 6). Although the spatial resolution is not as fine for the spectrometer, primarily due to pixel size, the agreement in temperatures is to within 1%–2% of the peak temperature. This slight disagreement may come from a slight misalignment of the central hotspot with respect to the spectrometer slit as the temperatures measured by the spectrometer tend to be lower than those measured by the 4-color system.

The fourth material in our study, Pt, is often used as an internal calibration standard for laser-heated DAC experiments due to its relative inertness.[5,26] However, its lower melting temperature (2045 K) and consequently lower blackbody emission intensity required longer exposure times, and thus longer heating times, to collect a sufficient signal above the stray light background to confidently measure temperature (see discussion of background subtraction above). However, we observe that the response of Pt to laser heating, whether by CW or flash, is slow (requiring a few seconds to heat up and stabilize); thus, a steady thermal emission is not possible with flash heating. Additionally, Pt is also prone to thermal runaway after several seconds of CW heating while melted. Therefore, we employ a different method to measure Pt using two different exposure times, one short corresponding to flash time scales (100 ms) and one long corresponding to CW times scales (2 s). Each exposure time required CW heating for a few seconds to allow the thermal emission to stabilize as determined by photodiodes that monitor the laser and thermal emission, respectively. Prior to thermal runaway, each sample

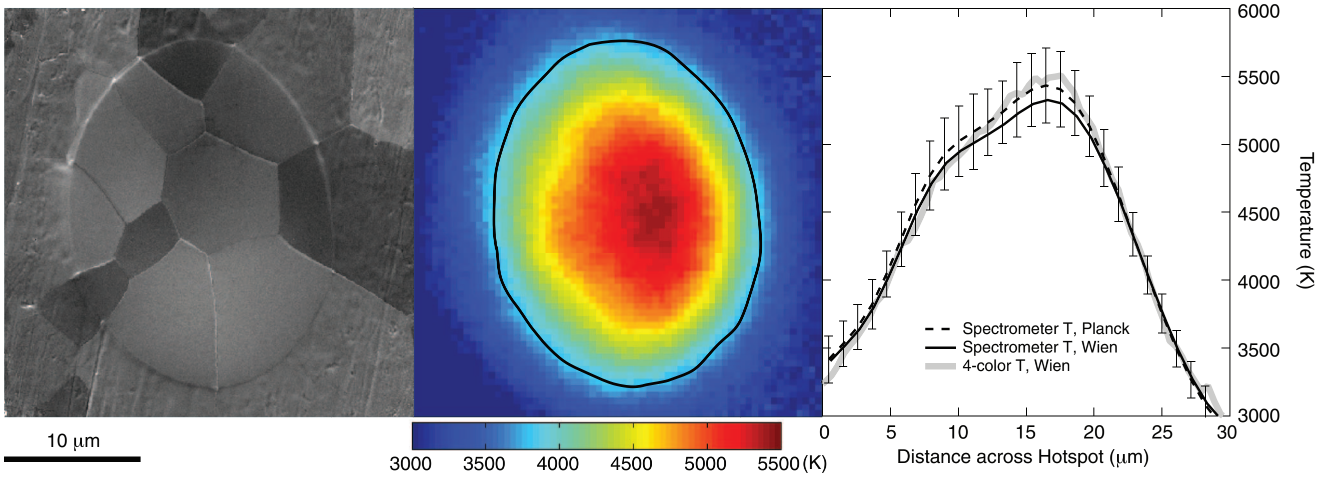

FIG. 6. (Left) SEM image and (center) corresponding temperature map of melted W with (Right) corresponding temperature transects across the center of flash-heated W at room pressures as collected by spectrometer (black curves) and by 4-color (thick gray curve) measurement systems. Solid lines are temperatures calculated using the Wien approximation, while the dashed line corresponds to a Planck fit of the spectrometer measurement. Note the very good agreement between the Planck and Wien fits for both measurement systems below ∼5000 K. The error bars shown are computed for the Planck fit of the spectrometer data and are an uncertainty determined by the 2-color pyrometer method.[4,28]

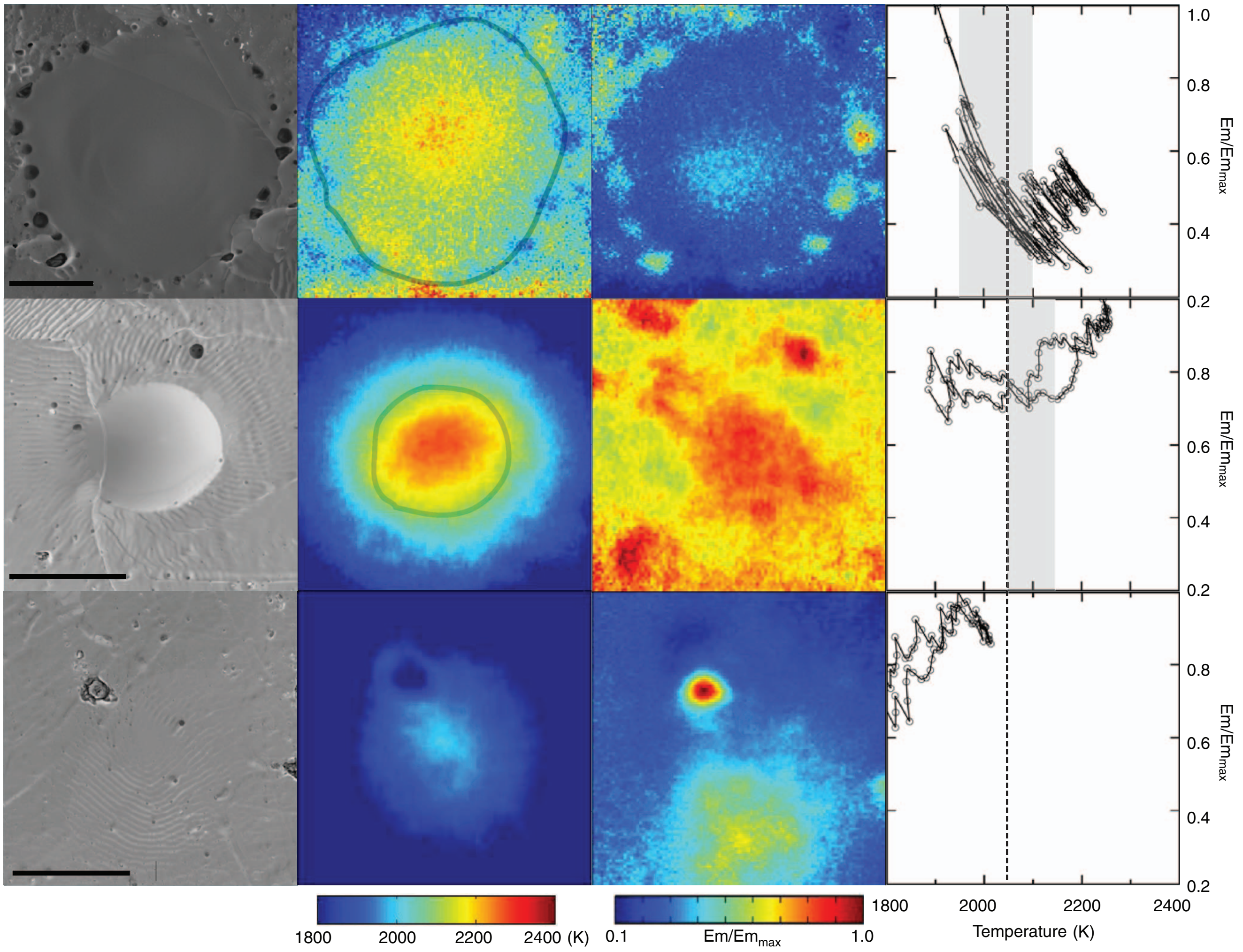

FIG. 7. (Far left) SEM images, (mid left) corresponding temperature maps, (mid right) emissivity maps, and (far right) emissivity versus temperature for a horizontal transect across the center of each map of CW-heated Pt samples. Melted Pt sample collected with 100 ms (top row) and 2 s exposure times (middle row), respectively. (Bottom row) Unmelted Pt collected with a 2 s exposure. The outlines shown on each temperature map correspond to the melt bleb features observed in the SEM images. The maximum temperature in each of the temperature maps is approximately 2250 K, 2250 K, and 2000 K from top to bottom row, respectively. The vertical line shown in the far-right column corresponds to the literature melting temperature value of Pt (2045 K). The shaded bands give the melting temperature and uncertainties as inferred from the temperature maps. Scale bars are each 20 μm.

is quenched just following temperature measurement, thus the texture recorded in the sample corresponds to the temperature measured. We vary the laser power to measure temperatures above and below the melting temperature for both heating exposure durations (Fig. 7). With the much longer exposure of 2 s, the signal-to-noise ratio is reduced dramatically, resulting in a much smoother temperature map.

There are differences, however, that are observed in the corresponding emissivity maps and emissivity versus temperature transects. Notably, Campbell[5] inferred a discontinuous jump in emissivity versus temperature yields the melting temperature, assuming emissivity is a material property that changes with melting. A discontinuity is not, however, observed for any of our flash-heated melted samples (i.e., Mo, Re, and W), although is observed for the long-duration measurement of CW heating of Pt (Fig. 7, center row, right). The SEM images for both melted samples of Pt show evidence of a melted bleb. This discrepancy in the emissivity maps suggests that although a discontinuity in emissivity (versus temperature) may be used to identify melt, it may not be due to specifically melting alone, but may instead also indicate that the signal measured is due to fluid motion in the melted sample (Fig. 8). Pt heated for a long duration yields visible fluctuation of temperature and hotspot position (Fig. 8), thus when integrated over a long period of time, the emissivity *may* show discontinuous jumps between regions that were hotter than other regions due to a moving hotspot. Thus, care needs to be taken during interpretation of emissivity discontinuities and melting. Additionally, especially for samples prone to thermal runaway such as Pt, when a temperature is measured, the conditions when the sample is quenched are important when inferring the state of melting. Instead, we suggest that when using flash heating and subsequent analyses of quenched samples, a short temperature measurement immediately before quench will give the most accurate melting temperature.

High-pressure melting of rhenium

In order to validate this new method at high pressures, we melted Re at high pressures and compared our results to

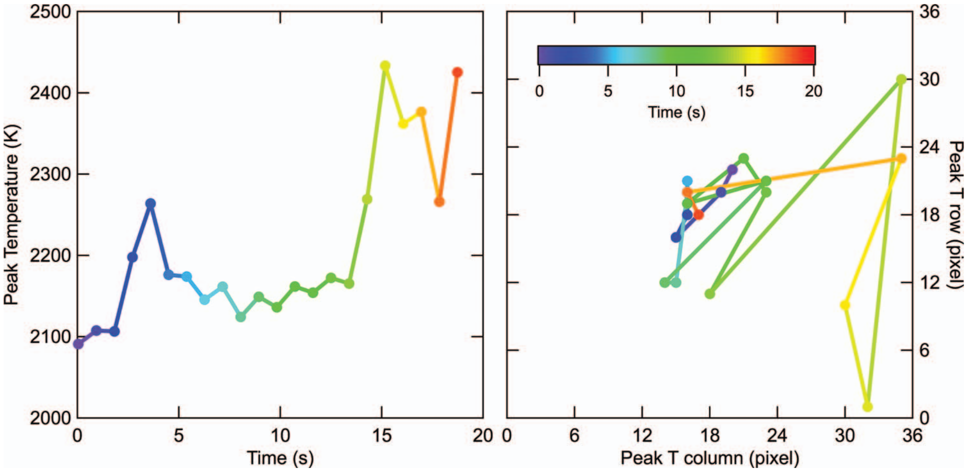

FIG. 8. Peak temperature and hotspot motion in CW-heated Pt after several seconds of heating at constant laser power. For all temperatures shown, Pt is melted. (Left) Peak temperature versus time taken at ∼1 s intervals with 40 ms exposure time. Between ∼5 and 14 s the peak temperature is relatively stable at ∼2150 K. Note that after ∼14 s, the temperature is no longer stable and begins to run away. (Right) Peak temperature position as a function of time. Note each pixel is ∼0.48 μm in dimension, thus motions up to ∼15 μm in 1 s are observed.

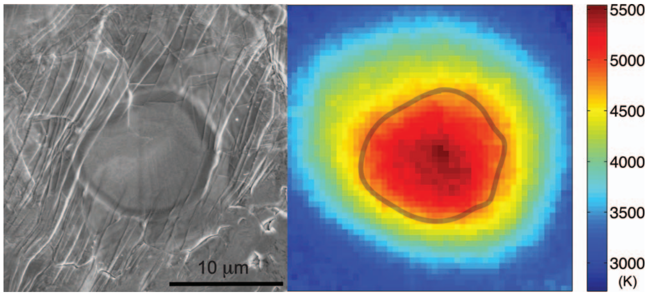

FIG. 9. (Left) SEM image and (right) corresponding temperature map of melted Re at 50 GPa. The outline shown on the temperature map corresponds to the melt bleb feature in the SEM image. The melting temperature inferred from this image is 4700 (± 300) K.

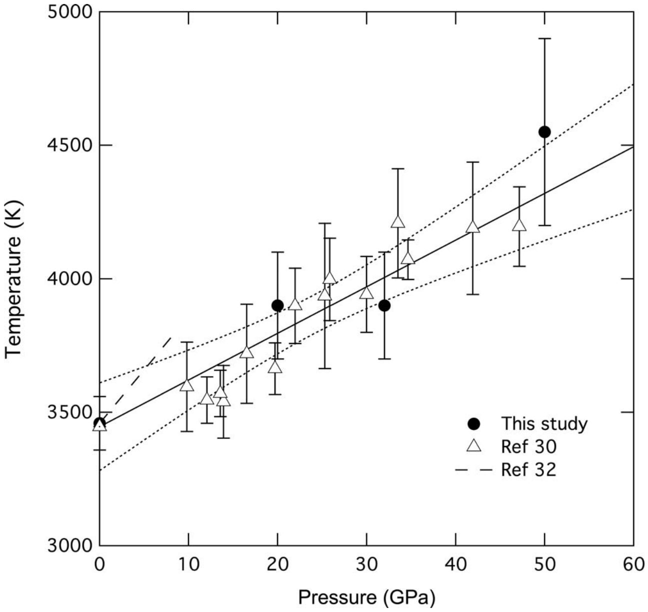

FIG. 10. High-pressure melting temperatures of Re as determined by this study (solid circles) as compared to a previous study at low pressures[32] (dashed line) and using flash heating[30] (open triangles). The solid line shows the best-fit curve to the previous data,[30] along with the 95% confidence bands given by the scatter of that data (dotted lines). The uncertainties shown here include differences between measurements as well as inherent uncertainties within a single measurement.

a recent flash-melted study of Re.[30] We loaded a cleaned, pre-compressed Re foil (∼12 μm thick) into the DAC and cryogenically filled the sample chamber with liquid argon to provide both thermal insulation and act as a pressure medium. We increased the pressure to the desired level as determined by Raman from the diamond culet.[31] Multiple (at least three) flash-melting experiments of 20 ms in duration were conducted on each sample at temperatures above and below the melting temperatures (Fig. 9). We get good agreement with previous flash-melted measurements[30] but less so with older measurements that were completed up to 8 GPa[32] (Fig. 10).

CONCLUSIONS

Fundamental observations of melting include the loss of rigidity and long-range order associated with the fluid state. Often, however, direct measurements of melting are experimentally precluded or obscured and indirect methods must be used instead. These melt proxies include changes in intrinsic optical (e.g., laser absorption, emission of blackbody radiation) or thermal properties (e.g., thermal conductivity), as well as extrinsic properties (e.g., surface roughness or quenched texture) of the sample. One or more of these proxies may be associated with melting, but one must be careful to test their reliability as experimental conditions change. In this study, we use the change in texture (formation of round blebs) as a proxy for melting, and find, at least in the metals we have tested, this to be a robust way to identify melting at room and high pressures at very high temperatures.

Thus, we have demonstrated a powerful new technique of *in situ* 2D temperature measurements under high quasi-hydrostatic pressures and *ex situ* texture and composition analysis of quenched samples by revision of the original 4-color design[5] that built upon the already extensive advantages of multi-wavelength imaging radiometry over earlier methods of temperature measurement in the laser-heated diamond-anvil cell. The added advantages of this new design are as follows:

1. Coupling multi-wavelength imaging with SEM measurements of the sample after flash heating yields a map of both morphological and chemical changes that can be directly compared to a temperature map. Consistency between morphology and temperature distribution confirms that the feature we infer as the melt boundary is correlated with temperature. The direct link of textural or chemical proxies for melting with temperature increases the reliability of this method.
2. New changes in the design (e.g., removal of pellicle beam splitters and redundant mirrors; and replacement of narrow-band filters) simplify alignment, increase flux, and improve overall image quality.
3. High-quality two-dimensional temperature maps using flash heating (>10 ms duration) are possible. Image quality is determined by the length of the laser pulse and the temperature.
4. Multiple and sequential short duration temperature maps are also possible for CW-heated samples, allowing for monitoring of temperature evolution.

ACKNOWLEDGMENTS

The authors would like to thank Andrew Campbell and Reinhard Boehler for technical advice, Zhenting Jiang for SEM measurements, and William Samela for machining assistance. We also thank Tim Pier (SPI Lasers), and the support staff at Agilent Technology. Z.D. and K.K.M.L. acknowledge the support from CDAC and National Science Foundation (NSF) (Grant No. EAR-0955824). The authors would also like to thank an anonymous reviewer for a critical assessment of this paper.

[1] A. Jayaraman, Rev. Mod. Phys. **55**(1), 65–108 (1983).
[2] L. R. Benedetti, D. Antonangeli, D. L. Farber, and M. Mezouar, Appl. Phys. Lett. **92**(14), 141903 (2008).
[3] L. R. Benedetti, N. Guignot, and D. Farber, J. Appl. Phys. **101**(1), 013109 (2007).
[4] L. R. Benedetti and P. Loubeyre, High Press. Res. **24**(4), 423–445 (2004).
[5] A. J. Campbell, Rev. Sci. Instrum. **79**, 015108 (2008).
[6] A. Kavner and T. S. Duffy, J. Appl. Phys. **89**(3), 1907–1914 (2001).
[7] A. Kavner and C. Nugent, Rev. Sci. Instrum. **79**(2), 024902 (2008).
[8] X. Y. Li, M. Manga, J. H. Nguyen, and R. Jeanloz, Geophys. Res. Lett. **23**(25), 3775–3778, doi:10.1029/96GL03648 (1996).
[9] M. Manga and R. Jeanloz, Geophys. Res. Lett. **23**(14), 1845–1848, doi:10.1029/96GL01602 (1996).
[10] M. Manga and R. Jeanloz, Geophys. Monogr. Ser. **101**, 17–25 (1998).
[11] W. R. Panero and R. Jeanloz, Rev. Sci. Instrum. **72**(2), 1306–1308 (2001).
[12] M. J. Walter and K. T. Koga, Phys. Earth Planet. Inter. **143**, 541–548 (2004).
[13] R. Jeanloz and A. Kavner, Philos. Trans. R. Soc. London, Ser. A **354**(1711), 1279–1305 (1996).
[14] R. Boehler and A. Zerr, Science **265**, 723 (1994).
[15] D. L. Heinz and R. Jeanloz, in *High Pressure Research in Mineral Physics*, edited by M. H. Manghnani and Y. Syono (AGU, Washington, DC, 1987), pp. 113–128.
[16] Q. Williams, E. Knittle, and R. Jeanloz, J. Geophys. Res. **96**, 2171–2184, doi:10.1029/90JB01999 (1991).
[17] R. Boehler and M. Ross, in *Treatise of Geophysics: Mineral Physics*, edited by G. D. Price (Elsevier, 2007), Vol. 2, p. 642.
[18] D. L. Heinz and R. Jeanloz, J. Geophys. Res. **92**(B11), 11437–11444, doi:10.1029/JB092iB11p11437 (1987).
[19] A. Zerr and R. Boehler, Science **262**, 553–555 (1993).
[20] E. Takahashi, J. Geophys. Res., [Solid Earth] **91**(B9), 9367–9382, doi:10.1029/JB091iB09p09367 (1986).
[21] A. Zerr, A. Diegler, and R. Boehler, Science **281**, 243–246 (1998).
[22] K. Hirose, Y. Fei, Y. Z. Ma, and H. K. Mao, Nature (London) **397**(6714), 53–56 (1999).
[23] G. Shen and P. Lazor, J. Geophys. Res. **100**(B9), 17699–17713, doi:10.1029/95JB01864 (1995).
[24] Z. M. Geballe and R. Jeanloz, J. Appl. Phys. **111**(12), 123518 (2012).
[25] J. A. Montoya and A. F. Goncharov, J. Appl. Phys. **111**(11), 112617 (2012).
[26] G. Shen, M. Rivers, Y. Wang, and S. Sutton, Rev. Sci. Instrum. **72**(2), 1273–1282 (2001).
[27] G. Y. Shen, V. B. Prakapenka, M. L. Rivers, and S. R. Sutton, Phys. Rev. Lett. **92**, 185701 (2004).
[28] A. Kavner and W. R. Panero, Phys. Earth Planet. Inter. **143**, 527–539 (2004).
[29] R. A. Fischer and A. J. Campbell, Am. Mineral. **95**, 1473–1477 (2010).
[30] L. Yang, A. Karandikar, and R. Boehler, Rev. Sci. Instrum. **83**, 063905 (2012).
[31] Y. Akahama and H. Kawamura, J. Appl. Phys. **100**(4), 043516 (2006).
[32] L. F. Vereshchagin, N. S. Fateeva, and M. V. Magnitskaya, JETP Lett. **22**(4), 106 (1975).